

Study of spin-Peierls transition in α' - NaV_2O_5 by infrared reflectivity

D. Smirnov^{a*}, P. Millet^b, J. Leotin^a, D. Poilblanc^c, J. Riera^d, D. Augier^c and P. Hansen^d

^aLaboratoire de Physique de la Matière Condensée, SNCMP-INSA, Complexe de Rangueil, 31077 Toulouse, France

^bCentre d'Elaboration de Matériaux et d'Etudes Structurales CNRS, BP 4347, 29 rue Jeanne Marvig, 31055 Toulouse, France

^cLaboratoire de Physique Quantique & UMR CNRS 5626, Université P. Sabatier, 31062 Toulouse, France

^dInstituto de Fisica Rosario, Consejo Nacional de Investigaciones Científicas y Técnicas y Departamento de Fisica,

Universidad Nacional de Rosario, Avenida Pellegrini 250, 2000-Rosario, Argentina

(December 2, 2024)

Polarized infrared reflectivity measurements have been performed on single crystals of the spin-Peierls compound α' - NaV_2O_5 in the temperature range 20–300 K. Pronounced spectral features associated with the formation of the dimerized phase were detected both in the **a**- and **b**-polarizations (perpendicular and parallel to the spin-1/2 chains, respectively). The temperature dependence of a salient spectral line at 718 cm^{-1} sharply rising below the transition temperature T_{SP} obeys a $(1 - T/T_{\text{SP}})^{2\beta}$ law with $T_{\text{SP}} \simeq 34.3 \text{ K}$ and $\beta \simeq 0.25$. In addition, a continuum signal is observed in the whole temperature range in the **a**-polarized optical conductivity spectra. In order to interpret these results, calculations of the static dimerization and of the optical conductivity based on a mean-field and a dynamical treatment of the lattice respectively are proposed.

78.30.Hv, 75.50.Ee, 63.20.-e, 64.70.Kb

The spin-Peierls (SP) transition has become a revived challenging effect in quasi-one dimensional magnetism since the recent discovery of two inorganic transition metal oxides compounds, first copper germanate CuGeO_3 (Ref. 1) and more recently sodium vanadate α' - NaV_2O_5 (Ref. 2). These compounds contain linear spin-1/2 chains coupled to three-dimensional phonons. At low temperatures this coupling leads to the SP phase transition characterized by a lattice dimerization together with the opening of a spin gap.

The revival of the subject already investigated before in numbers of organic salts³ is due to the availability of large size and high quality crystals offering the possibility to carry out relevant experiments like neutron, x-rays and Raman scattering, magnetic susceptibility, ESR, NMR, heat capacity, thermal expansion^{4–9}.

Optical spectroscopy is known to be a sensitive tool to investigate properties of magnetic compounds¹⁰ and provides a detailed knowledge of phonons, magnons and their fluctuation states. IR transmission experiments have been used to study the undistorted and SP phases in CuGeO_3 (Ref. 11). The SP phase of NaV_2O_5 has been recently studied by IR absorption in the frequency region 50 – 400 cm^{-1} . New absorption lines have been found to accompany the SP transition¹². Recently, the activation of a zone boundary phonon in the SP phase of CuGeO_3 has been observed as a new single tiny line in low temperature reflectivity spectra¹³. A distinctive feature of NaV_2O_5 in comparison with CuGeO_3 is the negligible magnetic interaction between the chains because of their isolation by V^{5+}O_5 non magnetic chains. Frustration ratios $\alpha \approx 0.24 \div 0.36$ (Ref. 14,15) have been suggested for CuGeO_3 and $\alpha \approx 0$ for NaV_2O_5 (Ref. 2). In addition, the nearest-neighbor intrachain exchange constant

$J \simeq 440 \text{ K}$ (Ref. 7), the transition temperature $T_{\text{SP}} = 35 \text{ K}$ and the spin gap $\Delta_{\text{spin}} = 79 \text{ cm}^{-1}$ in NaV_2O_5 are typically 3–4 times larger than in CuGeO_3 (Ref. 7). Also the dimerization δ , estimated in the adiabatic approximation from the $T = 0$ spin gap, has the value $\delta \simeq 0.014$ (Ref. 14) and $\delta \simeq 0.048$ (Ref. 16) for CuGeO_3 and NaV_2O_5 , respectively. Thus, the magneto-elastic coupling plays a larger role in NaV_2O_5 and enhanced spectral signatures of this coupling are expected in this system.

In the following, we report on infrared reflectivity measurements of NaV_2O_5 single crystals over frequencies between 100 and 10000 cm^{-1} and for temperatures between 20 and 300 K . The study focuses first on the room temperature display of the excitation spectrum for the incident polarization along the **a**- and **b**-axes. Then, prominent new lines giving salient evidence of the dimerized phase below 34 K are reported. A detailed study of the temperature dependence of the line at 718 cm^{-1} is presented. Finally, the outline of a calculation using Exact Diagonalization (ED) and Quantum Monte-Carlo (QMC) algorithms based on a mean-field or a dynamical treatment of the lattice is given.

High-quality single crystals NaV_2O_5 with size up to $2.7 \times 5.1 \times 0.3 \text{ mm}^3$ were prepared according to the procedure described in Ref. 17. The samples were characterized by magnetic susceptibility measurements performed with a SQUID magnetometer at $3 \text{ K} \leq T \leq 350 \text{ K}$.

The optical measurements were done with a Bruker IFS 113V spectrometer at nearly normal incidence of infrared radiation polarized along the **a**- and **b**-axes and $\mathbf{k} \parallel \mathbf{c}$. Room temperature transmission and reflection infrared spectra were measured in a spectral range between 90 and 10000 cm^{-1} with a resolution ranging from 1 cm^{-1} in the far-infrared region to 5 cm^{-1} in the near-infrared

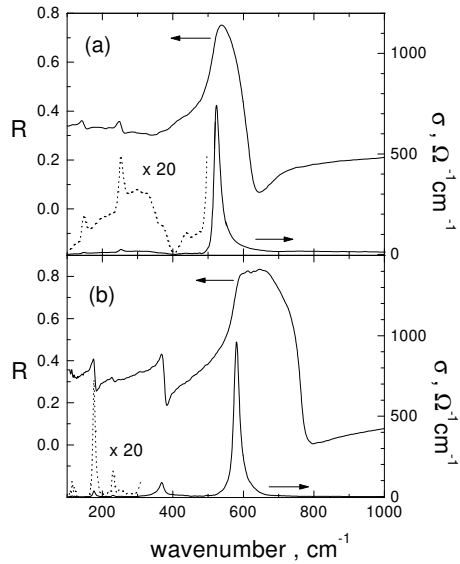


FIG. 1. Room temperature reflectivity spectra and optical conductivity of NaV_2O_5 single crystal for **a**-axis (a) and **b**-axis (b) polarizations.

region. The low temperature far-infrared spectra were measured with a continuous He flow cryostat down to 20 K with the absolute accuracy of temperature control about 0.1 K. The spectral range was $90\text{--}700\text{ cm}^{-1}$ for **a**-polarization and $90\text{--}1000\text{ cm}^{-1}$ for **b**-polarization with the resolution 1 cm^{-1} .

We can distinguish three different regions in the measured infrared spectra of NaV_2O_5 at 300 K. A rich phonon structure at frequencies below 1000 cm^{-1} is followed by transmission windows at $1500\text{--}5150\text{ cm}^{-1}$ for **a**-polarization and at $1120\text{--}5320\text{ cm}^{-1}$ for **b**-polarization. At higher frequencies, a wide maximum centered at approximately 7100 cm^{-1} was observed in the **a**-polarized reflectivity spectra. We have here restricted the discussion to the phonon part of the spectra.

In Fig. 1 the room temperature **a**- and **b**-axes reflectivity spectra (R) and the frequency-dependent conductivity (σ) derived via Kramers-Kronig analysis are shown in the region of lattice vibration frequencies up to 1000 cm^{-1} . Three phonons are detected for the **a**-polarization ($\omega_{TO} \approx 524, 251, 145\text{ cm}^{-1}$) and four for the **b**-polarization ($\omega_{TO} \approx 581, 367, 229, 175\text{ cm}^{-1}$). **b**-axis polarized reflectivity spectra have a typical form of phonon bands in an insulator which manifests in dynamical conductivity as Lorentzian peaks. Obvious features in the **a**-polarized σ spectrum are the occurrence of a broad excitation band ending at 400 cm^{-1} and an asymmetric line at 524 cm^{-1} with an underlying continuum extended above 1000 cm^{-1} (Fig. 1a). However, since the line shape depends strongly on the high- ω approximation

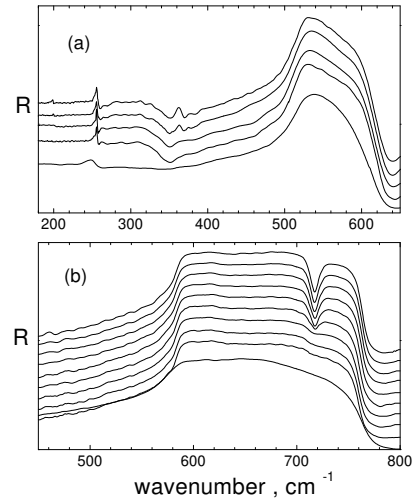


FIG. 2. Detailed temperature dependence in the reflectivity of $\alpha'\text{-NaV}_2\text{O}_5$ single crystal. (a)- $\mathbf{E} \parallel \mathbf{a}$, temperatures from up to down: 25, 29, 32, 37, 300K. (b)- $\mathbf{E} \parallel \mathbf{b}$, temperatures from up to down: 21.8, 24, 27.1, 29.5, 32, 33.5, 34.3, 35.3, 38, 300K. Spectra are shifted for clarity.

of the data ($> 10000\text{ cm}^{-1}$), reflectivity measurements in the visible and ultraviolet regions are necessary for a definite analysis.

Below T_{SP} , a pronounced modification of the reflectivity spectra is observed with sharply rising new features at $363, 200\text{ cm}^{-1}$ ($\mathbf{E} \parallel \mathbf{a}$), 718 cm^{-1} ($\mathbf{E} \parallel \mathbf{b}$) and 138 cm^{-1} (the polarization is unknown because of a poor signal-to-noise ratio in the very far-infrared region). The **a**-axis polarized broad band at $\omega < 400\text{ cm}^{-1}$ is enhanced at low temperatures, but neither the position nor the intensity changes at $T = T_{SP}$ (Fig. 2).

We performed a careful investigation of the 718 cm^{-1} line in the conductivity over temperatures between 20 and 38 K since this line is clearly associated to the lattice transformation at $T < T_{SP}$ (Fig. 3). At low temperatures ($T=21.8, 24, 27\text{ K}$) this peak is well described as a single Lorentz line with a constant linewidth. On the other hand, above 29 K the line profile is well described as superposition of a temperature-dependent Lorentz peak on top of a temperature-independent asymmetric broad line which can be clearly seen at 35.3 K and 38 K. This broad line might well be the signature of structural fluctuations growing in the vicinity of T_{SP} . Indeed, after subtraction of the temperature-independent part, a perfect Lorentz line with constant linewidth ($8.2 \pm 0.5\text{ cm}^{-1}$) is obtained for all T below the transition. We believe that the Lorentz-type line corresponds to a folded zone boundary phonon mode activated by the structural distortion and, therefore, the intensity of this line should be proportional to the squared dimerization. The tem-

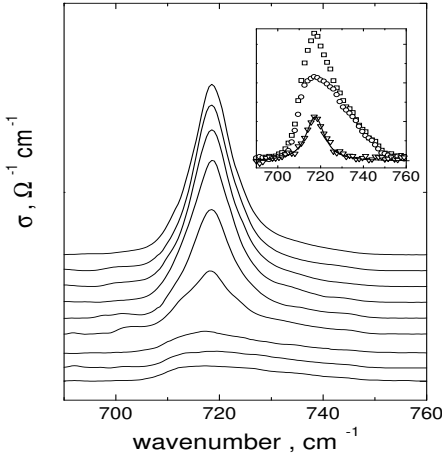


FIG. 3. Temperature evolution of the peak at 718 cm^{-1} (temperatures from up to down: 21.8, 24, 27.1, 29.5, 32, 33.5, 34.3, 35.3, 38 K) observed for a **b**-axis polarization. Spectra are shifted for clarity. The insert illustrates the correction procedure, as described in the text (\square : 34.3K, \circ : 38K, ∇ : difference, line: Lorentzian fit).

perature dependence of the normalized line intensity is shown in Fig. 4 as well as the result of a fit with the $(1 - T/T_{SP})^{2\beta}$ law. This fit in the temperature range 30–35 K gives $T_{SP}=(34.3\pm 0.2)$ K, $\beta=0.25\pm 0.1$.

We proceed now to discuss the above results in the context of existing theoretical approaches. The crudest description of the spin-Peierls ground state (GS) is based on the dimerized Heisenberg model: the antiferromagnetic coupling between nearest neighbor spins is assumed to be *statically* modulated (see Eq. (2) below) along each spin-1/2 chain. In fact, the physical origin of such a modulation relies on the *dynamical* magneto-elastic coupling. One of the simplest model including dynamical effects of phonons read^{18–20} (omitting the chain index),

$$H = J \sum_i (1 + \lambda u_i) \mathbf{S}_i \cdot \mathbf{S}_{i+1} + H_{\text{ph}}^0 + H_{\text{elastic}}^{\perp}, \quad (1)$$

where λ is the magneto-elastic coupling constant and u_i correspond to atomic displacements which modulate the exchange integral J . Here, we restrict ourselves to a single polarization of the phonon modes. Assuming independent optical phonons, the phonon hamiltonian takes the usual form, $H_{\text{ph}}^0 = \sum_i \left\{ \frac{p_i^2}{2M} + \frac{1}{2} K_{\parallel} u_i^2 \right\}$. An inter-chain elastic coupling $H_{\text{elastic}}^{\perp}$ is required to account for the three-dimensional coherence of the phonons and involves an additional elastic coupling K_{\perp} between neighboring chains. $H_{\text{elastic}}^{\perp}$ is needed to obtain a finite value of T_{SP} . Note that K_{\parallel} and λ depend strongly on the actual direction in space of the displacements u_i which is not explicitly specified in (1) (Ref. 21).

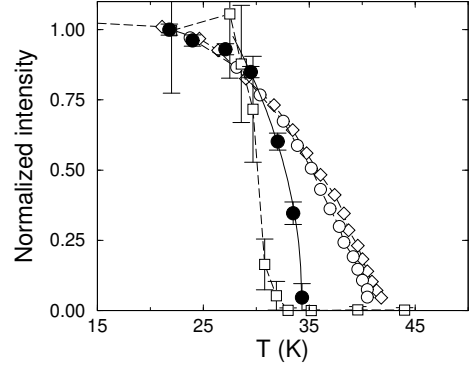


FIG. 4. Temperature dependence of the normalized squared dimerization obtained by ED (14 (\diamond), 16 (\circ) sites), QMC (\square , 40 sites) and intensity for the phonon mode observed at 718 cm^{-1} in **b**-axis polarization (\bullet). The solid line is a fit to a $(1 - T/T_{SP})^{2\beta}$ law. Error bars are shown for the QMC and experimental data.

The optical conductivity is theoretically defined as the GS correlation $\sigma(\omega) \propto \langle A_{IR}^{\dagger}(\omega + i0^+ - H)^{-1} A_{IR} \rangle_0$ where the operator $A_{IR} = \sum_i A_i$ describes the coupling between the ($\mathbf{q} = 0$) photons and the medium. Quite generally, one expects $A_i \propto E^{\alpha} u_i^{\beta} T_{\alpha\beta}(i)$, where \mathbf{E} is the electric field of the light, \mathbf{u}_i is the polarization of the phonon mode and $T_{\alpha\beta}(i)$ is the IR tensor which might include local spin fluctuations²².

In lowest order, A_{IR} corresponds to the emission of a $\mathbf{q} = 0$ phonon *i.e.* $T_{\alpha\beta}(i) = \delta_{\alpha\beta}$. According to Ref. 12, at $T > T_{SP}$ there are 15 $\mathbf{E} \parallel \mathbf{a}$ and 7 $\mathbf{E} \parallel \mathbf{b}$ phonons which should be active in the first order IR processes. We did not observe all the predicted modes probably because some of them have small oscillator strengths. The group theoretical analysis in the SP phase is not available yet.

Calculated optical conductivity spectra ($T = 0$) obtained by ED of a $N=12$ site ring are shown in Fig. 5 for a typical phonon frequency $\Omega = J$ and several values of the dimensionless coupling constant $g = \lambda/\sqrt{2M\Omega}$ ($H_{\text{elastic}}^{\perp}$ is neglected here and a variational basis is used for the phonons²⁰). As shown in the insert, the spin gap (and hence the dimerization) increases strongly with the coupling g . The doubling of the unit cell leads to an additional peak in $\sigma(\omega)$ corresponding to a new $\mathbf{q} = 0$ phonon mode at higher energy resulting from a folding of the Brillouin zone. This mechanism can then explain the experimental observation of the new line at 718 cm^{-1} if one assumes that the atomic displacements u_i have a component along the chains direction (**b**-axis).

As suggested theoretically²² and observed experimentally²³, higher order processes involving one phonon and two-magnon scattering can also take place with, e.g., an IR tensor like $T_{\alpha\beta}(i) = \mathbf{S}_i \cdot \mathbf{S}_{i+1} (\delta_{\alpha\beta} - \mathbf{e}_\alpha^{i,i+1} \mathbf{e}_\beta^{i,i+1})$, where $\mathbf{e}^{i,i+1}$ is the unit vector along the chain direction. In this case, the maximum absorption would occur for \mathbf{E} polarized along \mathbf{a} . A continuous background is indeed

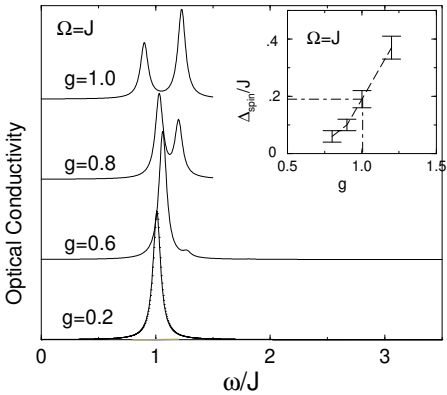


FIG. 5. Optical conductivity vs frequency calculated within model (1) for $\Omega/J = 1$ and for various spin-phonon coupling strengths g . Insert: Δ_{spin}/J vs g .

observed for such a geometry (see Fig. 1(a)) and could be associated to a two magnon phonon assisted absorption. More detailed theoretical and experimental investigations of this effect are left for a future study.

Although the treatment of the phonon dynamics at finite T is beyond the scope of this work, a simpler mean field treatment of the lattice is justified if the relevant phonons have a pronounced 3D character (*i.e.* K_{\perp} is not too small compared to K_{\parallel}) and if $\Omega/J \lesssim 1$. In the adiabatic approximation (which corresponds, strictly speaking, to the limit $\Omega/J \rightarrow 0$) the hamiltonian reads¹⁴,

$$H_{MF} = J \sum_i (1 + (-1)^i \delta) \mathbf{S}_i \cdot \mathbf{S}_{i+1} + \frac{1}{2} N K \delta^2, \quad (2)$$

where N is the number of sites, K an effective elastic constant and $\delta = \delta(T)$ the static dimerization which depends on the system size. The value of $\delta(T)$ is obtained by minimizing the total free energy $F_T = F_{\text{spin}}(T, \delta) + \frac{1}{2} N K \delta^2$, where F_{spin} corresponds to the spin part of hamiltonian (2). The zero temperature value $\delta(0) \simeq 0.048$ is imposed by the actual value of the ratio $\Delta_{\text{spin}}/J \simeq 0.2$ known from experiments⁷. The value of $\delta(T = 0)$, in turn, enforces the value of the ratio $K/J \simeq 3$. Note that K and J are the only two free parameters of the model ($J \simeq 440$ K is determined from a fit of the high- T spin susceptibility⁷) and, hence, the theoretical value for T_{SP} comes as an output of the model. The QMC calculation suggests $T_{\text{SP}} \simeq 33$ K, a value very close to the experimental one. The explicit temperature dependence $\delta^2(T)$ obtained by ED and QMC techniques²⁴ agrees reasonably with the experimental data, as shown in Fig. 4, apart from the value of the critical exponent²⁵.

In summary, we have studied the infrared reflectivity on NaV_2O_5 single crystals at temperatures down to 20K. The SP transition order parameter was measured through the phonon spectrum temperature dependence. These results are compared with calculations based on mean field or dynamical treatments of the lattice.

We acknowledge A. Damascelli and D. van der Marel for communicating their results of a similar study prior to publication.

* Permanent address: A. F. Ioffe Physical Technical Institute, 194021 St. Petersburg, Russia

¹ M. Hase *et al.*, Phys. Rev. Lett. **70**, 3651 (1993).

² M. Isobe and Y. Ueda, J. Phys. Soc. Jpn. **65**, 1178 (1996).

³ For a review on organic SP systems see e.g. J. W. Bray, L. V. Interrante, I. S. Jacobs and J. C. Bonner, in *Extended Linear Chain Compounds*, edited by J. S. Miller (Plenum Press, New York, 1983), Vol. **3**.

⁴ For a review on CuGeO_3 see e.g. J. P. Boucher and L. P. Regnault, J. Phys. I (Paris) **6**, 1939 (1996).

⁵ T. Ohama *et al.*, J. Phys. Soc. Jpn. **66**, 23 (1997).

⁶ T. Ohama *et al.*, J. Phys. Soc. Jpn. **66**, 545 (1997).

⁷ M. Weiden *et al.*, Z. Phys. B **103**, 1 (1997).

⁸ Y. Fujii *et al.*, J. Phys. Soc. Jpn. **66**, 326 (1997).

⁹ S. A. Golubchik *et al.*, cond-mat/9711048 (unpublished).

¹⁰ M. Cottam and D. Lockwood, *Light Scattering in Magnetic Solids* (John Wiley & Sons, New York, 1986)

¹¹ P. H. M. Van Loosdrecht, cond-mat/9711091 (unpublished).

¹² M. N. Popova *et al.*, Pis'ma v ZhETF **65**, 711 (1997).

¹³ A. Damascelli *et al.*, cond-mat/9708026 (unpublished); A. Damascelli *et al.*, cond-mat/9707155 (unpublished).

¹⁴ J. Riera and A. Dobry, Phys. Rev. B **51**, 16 098 (1995); A. Feiguin *et al.*, Phys. Rev. B **56**, 14 607 (1998).

¹⁵ G. Castilla *et al.*, Phys. Rev. Lett. **75**, 1823 (1995).

¹⁶ D. Augier, D. Poilblanc, S. Haas, A. Delia and E. Dagotto, Phys. Rev. B **56**, R5732 (1997).

¹⁷ M. Isobe *et al.*, submitted to J. Cryst. Growth (1998).

¹⁸ D. Khomskii, W. Geerstma and M. Mostovoy, Czech. J. of Phys. **46**, Suppl S6, 32 (1996).

¹⁹ I. Affleck, proceedings of the NATO ASI “*Dynamical Properties of Unconventional Magnetic Systems*”, April 97, preprint cond-mat/9705127, to be published.

²⁰ D. Augier, D. Poilblanc, E. Sørensen and I. Affleck, submitted to Phys. Rev. Lett. For results using a truncation procedure in momentum space see also D. Augier and D. Poilblanc, Eur. Phys. J. B **7**, in press (1998).

²¹ The dimerization δ can be defined within this model by $\delta^2 = \lambda^2 \lim_{N \rightarrow \infty} \frac{1}{N} \sum_r \langle u_i u_{i+r} \rangle (-1)^r$.

²² T. Moriya, J. Appl. Phys. **39**, 1042 (1968); see also J. Lorenzana and G. A. Sawatzky, Phys. Rev. B **52**, 9576 (1995) and J. Lorenzana and R. Eder, Phys. Rev. B **55**, R3358 (1997).

²³ H. Suzuura, H. Yasuhara, A. Furusaki, N. Nagaosa and Y. Tokura, Phys. Rev. Lett. **76**, 2579 (1996).

²⁴ ED deal with smaller rings than QMC and, hence, have larger finite size effects and overestimate T_{SP} .

²⁵ Deviations from the mean-field behavior ($\beta = 0.5$) have also been seen in CuGeO_3 ; see e.g. Ref. 13, L. P. Regnault *et al.*, Phys. Rev. B **53**, 5579 (1996) and M.C. Martin *et al.*, Phys. Rev. B **53**, 14713 (1996).